



# Electrochemical Behavior of Composite Nanoparticles on the Corrosion of Mild Steel in Different Media

A. M. Abdel-Gaber<sup>1</sup> · R. Awad<sup>2</sup> · H. T. Rahal<sup>1</sup> · D. Moussa<sup>2</sup>

Received: 28 November 2018 / Revised: 2 March 2019 / Accepted: 25 March 2019 / Published online: 3 April 2019  
© Springer Nature Switzerland AG 2019

## Abstract

$Zn_{0.97}Mn_{0.03}O$  and  $Zn_{0.87}Mn_{0.03}Fe_{0.1}O$  nanoparticles have been synthesized using co-precipitation technique. The obtained nanoparticles were characterized by X-ray diffraction, and transmission electron microscopy. The elemental contents of the prepared nanoparticles were determined using particle-induced X-ray emission. Besides, the oxygen content of these nanoparticles was determined using non-Rutherford backscattering spectroscopy. The electrochemical behaviour of 10 ppm nanoparticles on the corrosion of mild steel in 0.5 M HCl and 0.5 M NaCl solutions containing 1% SDS was studied using potentiodynamic polarization curve measurements and electrochemical impedance spectroscopy techniques. The mechanism of inhibition of the studied nanoparticles was discussed and explained. Iron containing nanoparticles enhanced the corrosion protection of mild steel in 0.5 M HCl due to the ability of  $Fe^{2+}$  to deposit onto metal surface. However, in neutral 0.5 M NaCl medium, both nanoparticles have approximately similar efficiency.

**Keywords** Mild steel · Nanoparticles · HCl · NaCl · Electrochemical behaviour · Corrosion

## 1 Introduction

Mild steel is highly exposed to deterioration and corrosion especially in acidic and neutral media. Hydrochloric acid is ordinarily used in many domains such as acid cleaning and descaling, as well as acid pickling due to its low cost and availability compared to other mineral acids [1–8]. In addition, seawater is aggressive for industrial installations of mild steel causing severe corrosion problems [9].

Mild steel has been widely used in several fields including petroleum refineries equipment, storage tanks and pipelines due to its ease of manufacture and low cost [1, 10–14]. The pipelines are affected by the flow of fluids containing suspended matter (nanoparticles) giving rise to erosion–corrosion or general wear [15]. In stagnant solutions, the presence

of such suspended particles may either enhance or retard the corrosion due to their unique properties and their ability to deposit on metallic surfaces. The properties of nanoparticles are based on their peculiar electronic configuration, large surface area and high amount of surface atoms [16]. Numerous nanoparticles have been used as corrosion inhibitors such as  $TiO_2$  [17],  $Cu_2O$  [18],  $ZnO$  [19] and  $Fe_3O_4$  [20] nanoparticles.

This work aims to evaluate the electrochemical behavior of 10 ppm of  $Zn_{0.97}Mn_{0.03}O$  and  $Zn_{0.87}Mn_{0.03}Fe_{0.1}O$  nanoparticles on the corrosion of mild steel in 0.5 M HCl and 0.5 M NaCl solutions using electrochemical impedance spectroscopy (EIS) and potentiodynamic polarization techniques.

## 2 Experimental Studies

### 2.1 Nanoparticle Preparation and Characterization

$Zn_{0.97}Mn_{0.03}O$  (ZnMnO) and  $Zn_{0.87}Mn_{0.03}Fe_{0.1}O$  (ZnMn-FeO) nanoparticles were prepared using co-precipitation technique as described previously [21].

X-ray diffraction (XRD) patterns of the prepared nanoparticles were obtained using the Bruker D8 advance powder diffractometer with Cu-K $\alpha$  radiation ( $\lambda = 1.54056 \text{ \AA}$ )

✉ A. M. Abdel-Gaber  
a.abdelgaber@bau.edu.lb

H. T. Rahal  
Hrhal@bau.edu.lb

<sup>1</sup> Department of Chemistry, Faculty of Science, Beirut Arab University, P.O. Box 11-50-20 Riad El Solh, Beirut 11072809, Lebanon

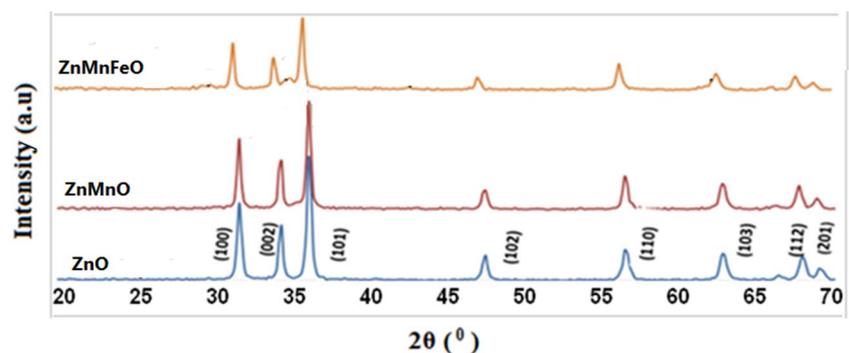
<sup>2</sup> Department of Physics, Faculty of Science, Beirut Arab University, Beirut, Lebanon

in the range  $10^\circ \leq 2\theta \leq 80^\circ$ . Transmission electron microscopy (TEM) images were obtained using Jeol transmission electron microscope JEM 100CX, operated at 80 kV. The size distribution was obtained from TEM images using ImageJ software and it was also done by Particle Analyzer Delsa™Nano UI Software Version 3.73. Both TEM and particle size samples were prepared from reaction solution and dispersed in ethanol solvent for measurement. The elemental composition of the samples was measured by the conventional vacuum PIXE. The 1.7 MV tandem accelerator of the Lebanese Atomic Energy Commission was used to deliver 3 MeV proton beam on the samples with 1  $\mu\text{C}$  of fluence. The GUPIX software that measures the weight concentrations of Zn, Fe and Mn, but not O as the latter is invisible with respect to PIXE technique. For Ion Beam Analysis, that is PIXE and RBS, a mass of 0.3 g of each sample was grinded very well to ensure homogeneity and hence a thick target pellet of approximate dimensions  $1 \times 1 \times 0.2 \text{ cm}^3$  was formed. The target chamber contains Silicon-drifted detector (SDD) formed of high purity silicon with a very low leakage current leading to high energy resolutions (down to 123 eV for Mn  $K\alpha$  wavelength). The SDD allows the detection of elements with  $Z > 10$ . To obtain one spectrum for all the elements which compose the sample, an Aluminum filter of 100  $\mu\text{m}$  thickness was placed in front of SDD X-ray absorber [22].

## 2.2 Solution Preparation

Distilled water as well as analytical reagent-grade hydrochloric acid were used without further purification to prepare the experimental solutions. Sodium chloride, as well as sodium dodecyl Sulfate (SDS) were purchased from Sigma-Aldrich. 1 wt% SDS was added to every test solution, either acidic or neutral media. SDS is considered as an excellent electrostatic stabilizer with high affinity to adsorb onto nanoparticle surfaces maintaining their stable dispersion [23]. To homogenize the resultant solution, a Bandelin Sonoplus ultrasonic stirrer solution was used for mixing the solution for 30 min.

**Fig. 1** XRD spectra for undoped ZnO, ZnMnO and ZnMnFeO nanoparticles



## 2.3 Electrochemical Studies

Electrochemical impedance spectroscopy (EIS) and potentiodynamic polarization measurements were done using frequency response analyzer (FRA)/potentiostat supplied from ACM instruments (UK). The frequency range for EIS measurements was  $0.1\text{--}3 \times 10^4 \text{ Hz}$  with applied potential signal amplitude of  $\pm 10 \text{ mV}$  around the rest potential. Polarization curves measurements were obtained at a sweep rate of  $1 \text{ mVs}^{-1}$ . In 0.5 M NaCl, the mild steel was polarized from  $-300$  to  $+500 \text{ mV}$  versus equilibrium potential, whereas in 0.5 M HCl solutions polarization curve measurements were done within a potential range of  $\pm 250 \text{ mV}$  around the rest potential. The used cell setup and conditions were similar to that described previously [24]. The mild steel used for constructing the working electrode was of the following chemical composition (wt%) (C, 0.164; Mn, 0.710; Si, 0.260; S, 0.001; P, 0.005 and Fe, 96.2). Before polarization and EIS measurements, the working electrode was left to attain the open circuit potential in the test solution. A WiseCircu water bath (Germany) was used to maintain the temperature of all measurements at  $30 \pm 0.1^\circ \text{C}$  under unstirred conditions. Duplicate experiments were performed, under the same conditions, to test the reliability and reproducibility of the measurements.

## 3 Results and Discussion

### 3.1 Nanoparticle Characterization

Figure 1 shows the XRD diffraction spectra for undoped ZnO, ZnMnO and ZnMnFeO nanoparticles. Comparing the observed diffraction peaks to the standard peaks of pure ZnO (ICDD card no. 89-1397), indicated that all samples show the hexagonal (wurtzite) crystal structure. The sharp and narrow peaks reveal that all prepared nanoparticles exhibit high purity and crystallinity [21].

High-resolution TEM images as well the size distribution of ZnMnO and ZnMnFeO nanoparticles are shown in Fig. 2a and b. As seen, uniform nanoparticles with narrow size distribution are obtained. Both nanoparticles exhibit a three-dimensional network of randomly oriented sheet-like structures. The TEM size distributions were obtained and the average particle sizes were determined from the histograms to be 25–45 nm for ZnMnO and 40–80 nm for ZnMnFeO nanoparticles, respectively.

The agglomeration appearing in TEM images is probably due to the fact that the measurements were carried in ethanol solvent without the use of capping agent.

Figure 3a and b shows the size distribution of the investigated nanoparticles using a  $10^\circ$  scattering angle. The

average particle size was 4.2 nm for ZnMnO and 27.7 nm for ZnMnFeO nanoparticles, respectively.

The concentration of Mn and Fe in  $\text{Zn}_{0.97}\text{Mn}_{0.03}\text{O}$  (ZnMnO) and  $\text{Zn}_{0.87}\text{Mn}_{0.03}\text{Fe}_{0.1}\text{O}$  (ZnMnFeO) nanoparticles has a noticeable effect on the structural, optical and magnetic properties. For this reason, it is very important to calculate the weight concentrations (wt%) of Zn, Mn, Fe and using PIXE and RBS. PIXE was used first to determine the weight concentrations of the elements in  $\text{Zn}_{0.97}\text{Mn}_{0.03}\text{O}$  (ZnMnO) and  $\text{Zn}_{0.87}\text{Mn}_{0.03}\text{Fe}_{0.1}\text{O}$  (ZnMnFeO) nanoparticles using the GUPIX software that measures the weight concentrations of Zn, Fe and Mn, but not O as the latter is invisible with respect to PIXE technique.

The stoichiometric concentrations of Zn, Fe and Mn were calculated using Eq. (1) and presented in Table 1.

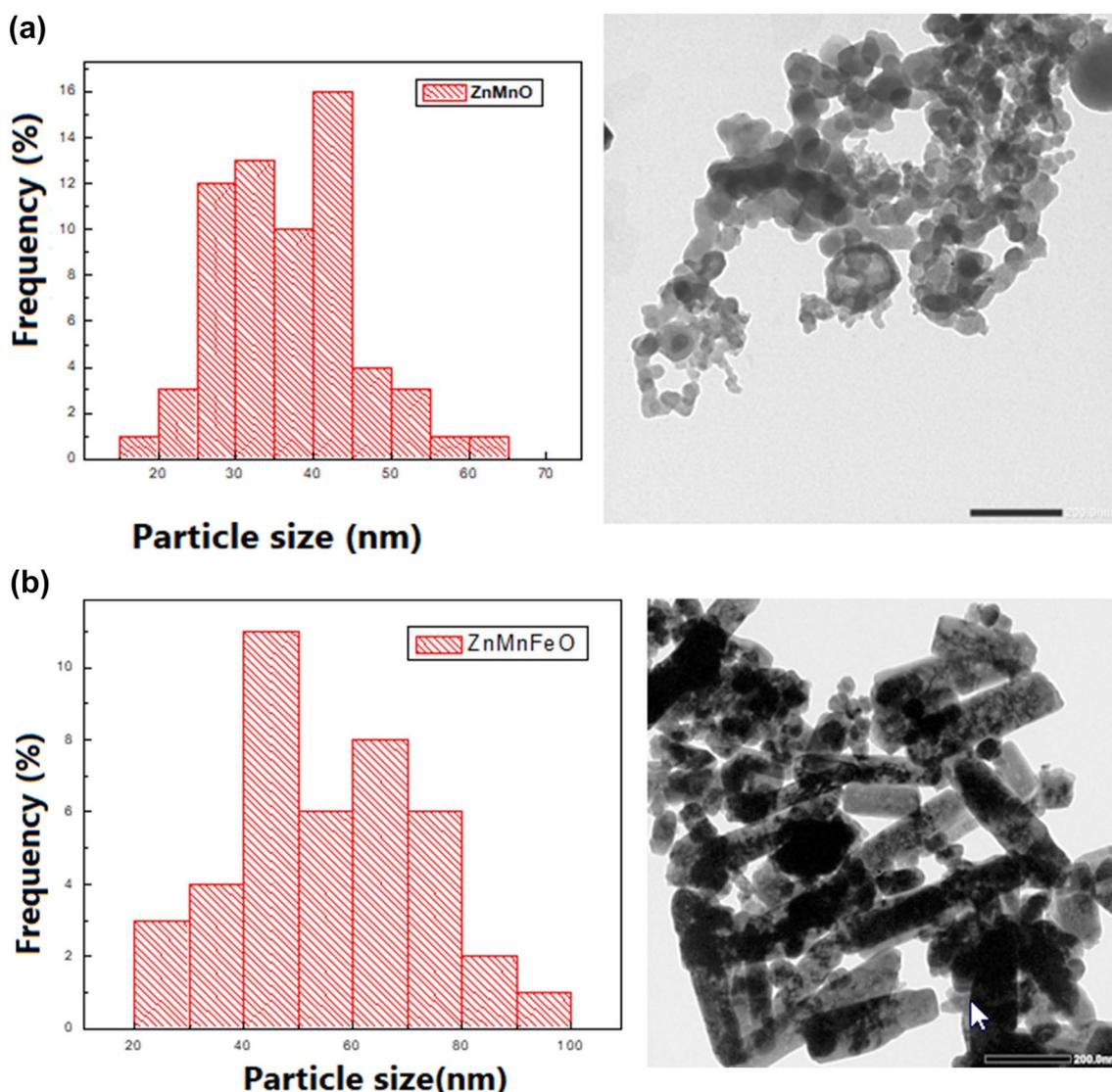
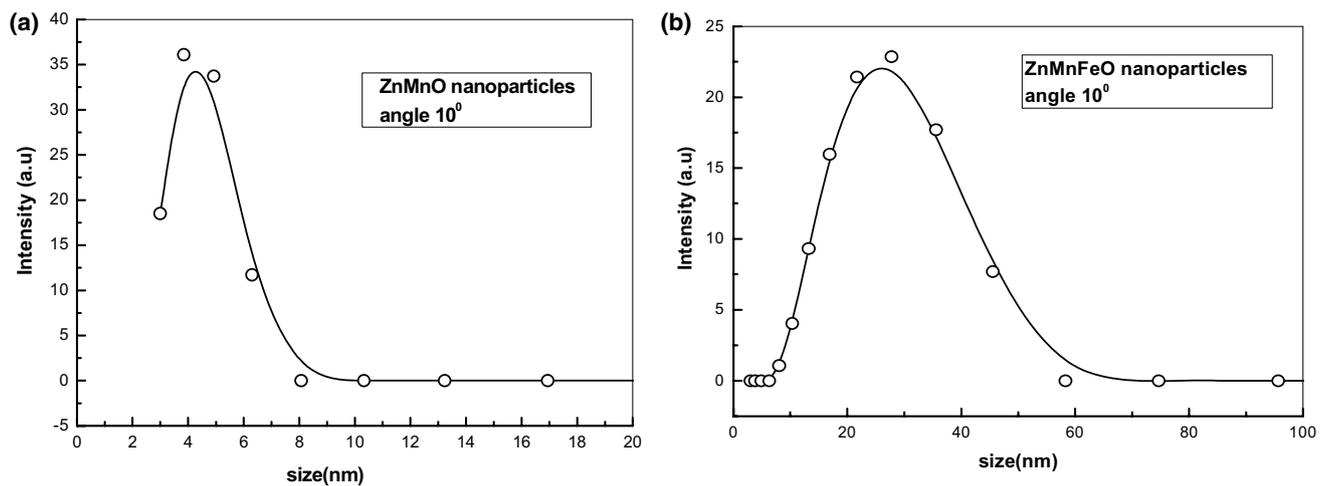


Fig. 2 TEM images and size distribution of ZnMnO (a) and ZnMnFeO nanoparticles (b)



**Fig. 3** a, b Particle size distribution for the tested nanoparticles at detection angle  $10^\circ$

**Table 1** The wt% and the stoichiometry of Zn, Mn, Fe and O in  $Zn_{0.97-x}Mn_{0.03}Fe_xO$  using PIXE

Nps	Element	Experimental (wt%)	Theoretical (wt%)	Error %	Stoichiometry
ZnO	Zn	80.21	80.14	0.087	1.00087
	Mn	0.00	0.005	–	–
	Fe	0.00	0.1	–	–
	O	18.71	18.6	0.58	1.00591
ZnMnO	Zn	78.2	78	0.25	1.00256
	Mn	2.0	1.9	5	1.05263
	Fe	0.00	0.12	–	–
	O	18.6	19.1	–2.6	0.96857
ZnMnFeO	Zn	70.7	71.5	–1.13	0.98881
	Mn	2.42	2.28	5.7	1.06140
	Fe	7.5	7.9	–5.33	0.94936
	O	17.6	17.5	0.56	1.00571

$$x_r = \frac{[(x_r^{wt\%}/100) \times M_{rT}]}{M_{rx}} \quad (1)$$

where  $x_r^{wt\%}$  is the real element-content as wt%,  $M_{rT}$  the total molecular weight and  $M_{rx}$  is the molecular weight of the element.

Figure 4a–c show the RBS spectra of ZnO,  $Zn_{0.97}Mn_{0.03}O$  (ZnMnO) and  $Zn_{0.87}Mn_{0.03}Fe_{0.1}O$  (ZnMnFeO) nanoparticles, respectively, using 3 MeV proton elastic backscattering by fitting a non-Rutherford backscattering cross-section for O [22, 25, 26] in the SIMNRA simulations. The actual O-content, as wt% and stoichiometric ratios, for all samples, was determined and listed in Table 2.

The tabulated data showed that PIXE and RBS techniques provided accurate measurements for Zn and Mn

contents with relatively low % error. However, regarding the oxygen content, RBS revealed that there is some oxygen vacancies in the ZnO matrix for all the samples due to the large error between the theoretical and experimental results (1.58–10.3%), which might be the evidence of the existence of ferromagnetic nature of pure ZnO as discussed in previous work [21].

## 3.2 Corrosion Behavior of ZnMnO and ZnMnFeO Nanoparticles on Mild Steel in 0.5 M HCl and 0.5 M NaCl

### 3.2.1 Potentiodynamic Polarization Measurements

Figures 5 and 6 show potentiodynamic polarization curves for mild steel in 0.5 M HCl and NaCl containing 1% SDS. It is clearly observed that the addition of 10 ppm nanoparticles suppresses both cathodic and anodic part of the polarization curves in both media. However, in 0.5 M NaCl the cathodic parts of the polarization curves represents limiting current of oxygen reduction, whereas the anodic part indicates active dissolution of mild steel.

The electrochemical polarization parameters, corrosion potential,  $E_{corr}$ , anodic and cathodic Tafel slopes,  $\beta_a$ , and  $\beta_c$ , and the corrosion current density,  $i_{corr}$ , obtained from these curves are depicted in Table 3.

The tabulated data revealed that the corrosion current density decreases in the presence of both nanoparticles. These observations explain that these nanoparticles have the ability to retard the corrosion of steel in acidic and neutral media. The slight variations in  $\beta_a$  and  $\beta_c$  and  $E_{corr}$  of the nanoparticles in hydrochloric acid solutions indicate that the

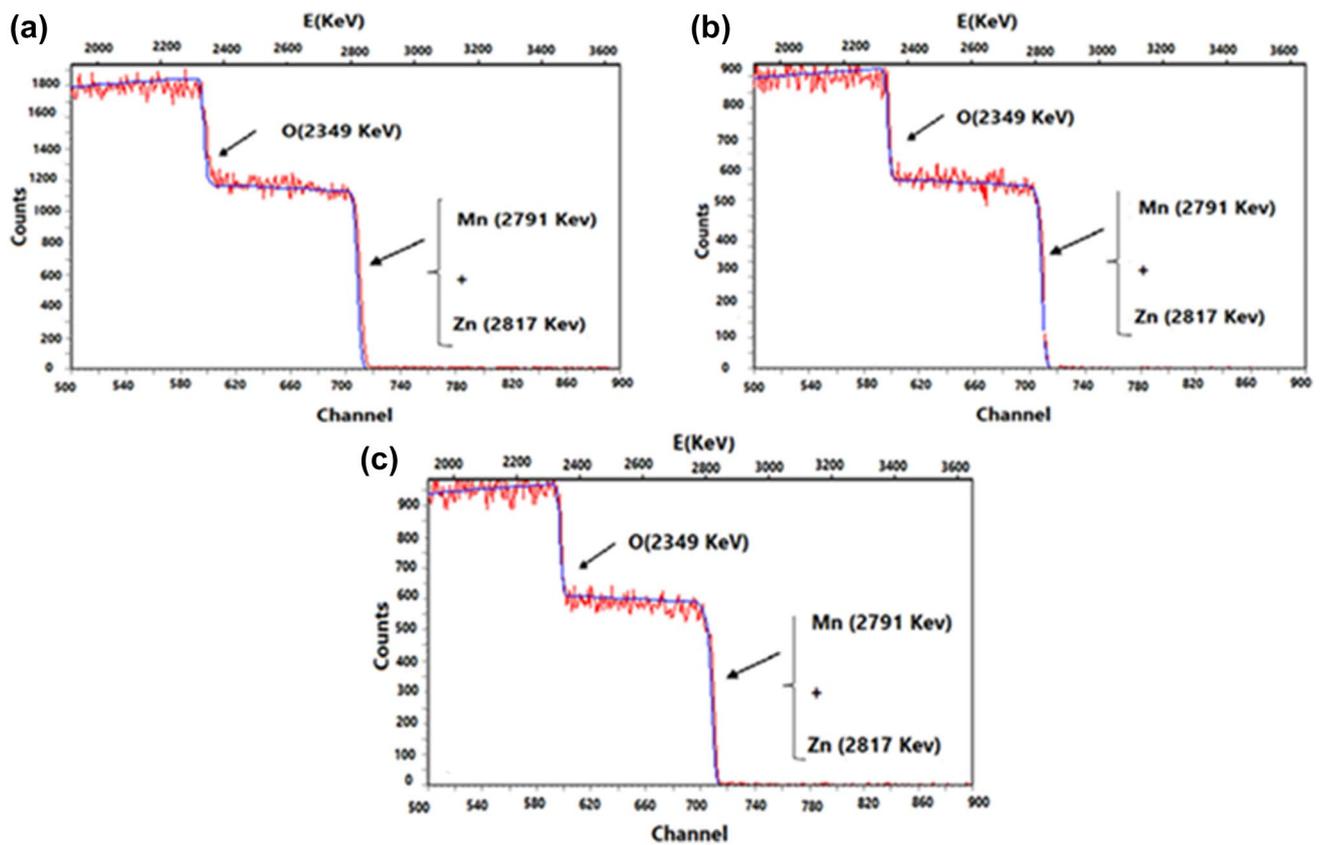


Fig. 4 a–c RBS spectra of ZnO, Zn<sub>0.97</sub>Mn<sub>0.03</sub>O (ZnMnO) and Zn<sub>0.87</sub>Mn<sub>0.03</sub>Fe<sub>0.1</sub>O (ZnMnFeO) nanoparticles

**Table 2** The wt% and the stoichiometry of Zn, Mn, Fe and O in the studied nanoparticles using RBS

Nps	Element	Experimental (wt%)	Theoretical (wt%)	Error %	Stoichiometry
ZnO	Zn	80.30	80.14	0.19	1.00199
	Mn	0.00	0.005	–	–
	Fe	0.00	0.1	–	–
	O	18.9	18.6	1.58	1.01612
ZnMnO	Zn	79.4	78	1.39	1.01415
	Mn	2.0	1.9	5	1.05263
	Fe	0.00	0.12	–	–
	O	18.5	19.1	–3.24	0.96858
ZnMnOFe	Zn	71.9	71.5	0.55	1.00559
	Mn	2.19	2.28	–4.1	0.96052
	Fe	8.3	7.9	4.8	1.05063
	O	16.3	17.5	–7.36	0.93142

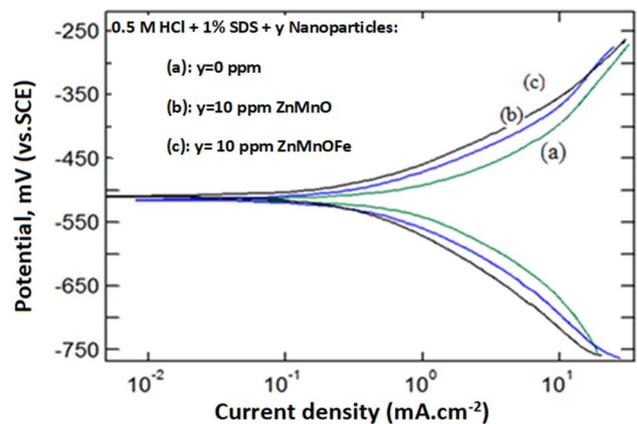
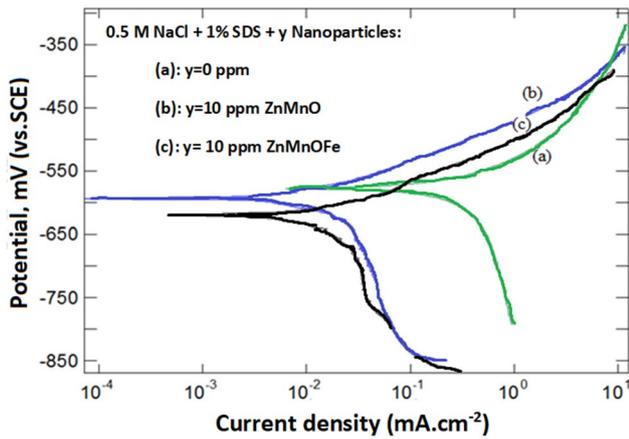


Fig. 5 Potentiodynamic polarization curves for mild steel in 0.5 M HCl containing 1% SDS in the absence and presence of 10 ppm of different additives of nanoparticles

inhibition process occurs without altering the mechanism [27]. The corrosion potential values of the nanoparticles in sodium chloride solutions were shifted to more negative



**Fig. 6** Potentiodynamic polarization curves for mild steel in 0.5 M NaCl containing 1% SDS in the absence and presence of 10 ppm of different additives of nanoparticles

values indicating the influence of these nanoparticles on the cathodic process.

### 3.2.2 Electrochemical Impedance Spectroscopy Measurements

The impedance plots shown in Fig. 7 consist of depressed semicircle of capacitive type indicating that the dissolution process of mild steel in 0.5 M HCl solution occurs under activation control [24, 28]. On the other hand, Fig. 8 indicates that the impedance plots of mild steel in 0.5 M NaCl consist of two overlapped depressed semicircles followed by diffusion tail indicating that the corrosion process occurs under diffusion control [29–31].

The impedance spectra for mild steel in 0.5 M HCl containing 1% SDS were analyzed by fitting the experimental data to a simple equivalent circuit model shown in Fig. 9 [32]. The circuit displayed in Fig. 10 was used to analyze the impedance plots of mild steel in 0.5 M NaCl containing 1% SDS. The circuits include the solution resistance ( $R_s$ ), constant phase element (CPE) that is placed in parallel to charge transfer resistance element ( $R_{ct}$ ), and a Warburg diffusion impedance ( $W$ ).

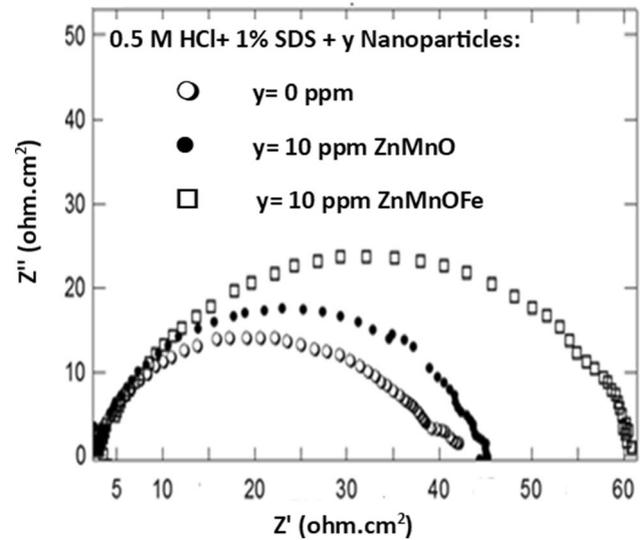


**Fig. 7** Nyquist impedance plots for mild steel in 0.5 M HCl containing 1% SDS in the absence and presence of 10 ppm of different additives of nanoparticles

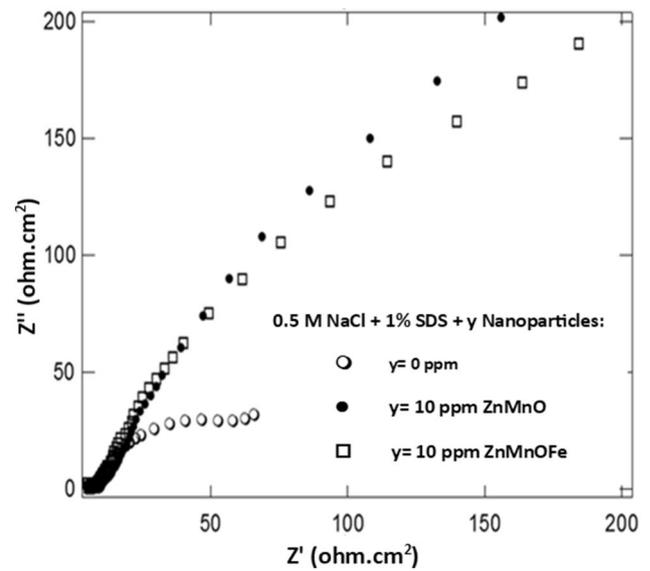


**Fig. 8** Nyquist impedance plots for mild steel in 0.5 M NaCl containing 1% SDS in the absence and presence of 10 ppm of different additives of nanoparticles

**Table 3** Potentiodynamic polarization parameters for mild steel in 0.5 M HCl and 0.5 M NaCl in the absence and presence of 10 ppm of different additives of nanoparticles

Medium	Additive	$E_{corr}$ (mV vs.SCE)	$\beta_a$ (mV/decade)	$\beta_c$ (mV/decade)	$i_{corr}$ (mA cm <sup>-2</sup> )
0.5 M HCl+1% SDS	–	– 508	91	103	0.39
	ZnMnO	– 505	95	80	0.37
	ZnMnFeO	– 509	86	110	0.33
0.5 M NaCl + 1% SDS	–	– 595	146	564	0.44
	ZnMnO	– 652	72	586	0.049
	ZnMnFeO	– 657	78	636	0.052

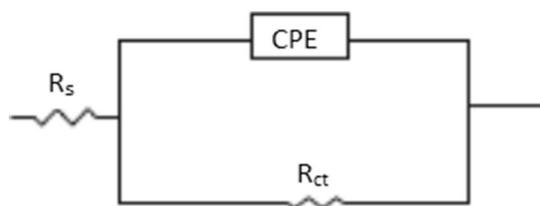


Fig. 9 Schematic for the equivalent circuit model used in HCl solutions

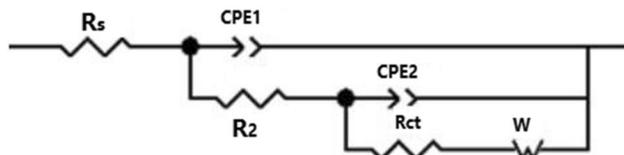


Fig. 10 Schematic for the equivalent circuit model used in NaCl solutions

The constant phase element (CPE) is defined by two values, the non-ideal double layer capacitance ( $Q_{dl}$ ) and constant ( $n$ ).

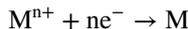
The values of electrochemical impedance parameters obtained from fitting of the experimental data of mild steel in 0.5 M HCl and 0.5 NaCl containing 1% SDS are presented in Table 4.

The  $R_{ct}$  values for mild steel in 0.5 M HCl solutions indicated that the addition of ZnMnFeO nanoparticles enhanced the corrosion protection of mild steel compared to ZnMnO nanoparticles. On the other hand, in 0.5 M NaCl, both nanoparticles exhibit similar effect. The decrease in  $(Q_{dl})_1$  values with respect to their corresponding blank could be attributed to the adsorption of nanoparticles over the metal surface [24].

The obtained data from polarization curve measurements are in a good agreement with those obtained from impedance measurements.

### 3.2.3 Inhibition Mechanism

The inhibition effect of 10 ppm ZnMnFeO and ZnMnO nanoparticles can be attributed to the adsorption or electrodeposition reaction of metallic cations on the mild steel surface showed by equation.



where  $M^{n+}$  could be  $Mn^{2+}$ ,  $Zn^{2+}$  or  $Fe^{2+}$  and  $n$  is the number of electrons contributing in the electrochemical reaction.

It was found that the presence of ZnMnFeO nanoparticles enhanced the corrosion protection of mild steel in acidic medium. Such behaviour is explained on the basis of the standard oxidation potential of different constituent metals of nanoparticles where,  $E_{Mn/Mn^{2+}} = 1.185$ ,  $E_{Zn/Zn^{2+}} = 0.7628$ ,  $E_{Fe/Fe^{2+}} = 0.44$  V. Thus, the low potential of Fe compared to Mn and Zn indicates the ability of  $Fe^{2+}$  to deposit onto mild steel surface.

It was reported that mild steel surface in HCl solution is positively charged [24], so  $Fe^{2+}$  ions will deposit through a close-packed triple layer in which negative  $Cl^-$  ions will get first adsorbed on the steel surface, followed by positively charged  $Fe^{2+}$  ions. In neutral 0.5 M NaCl medium, it was found that ZnMnO is hardly more efficient in protection of mild steel. This could be explained on the basis of Pourbaix diagram of iron [33]. In neutral medium (pH 7), The Fe nanoparticles exist in the form of  $Fe^{3+}$ , with  $E_{Fe/Fe^{3+}} = 0.04$  V. The deposition of  $Fe^{3+}$  over mild steel surface in neutral media forms rust  $Fe_2O_3 \cdot H_2O$  which is none adherent porous corrosion product. In such case, rust does not prevent corrosion and the corrosion rate proceed in linear rate.

## 4 Conclusion

ZnMnFeO and ZnMnO nanoparticles retard the corrosion of mild steel in acidic and neutral media. ZnMnFeO nanoparticles were more efficient in acidic media rather than in neutral media due to the ability of  $Fe^{2+}$  to deposit onto metal surface. However, in neutral 0.5 M NaCl medium, both nanoparticles carry analogous efficiencies.

Table 4 Electrochemical impedance parameters for mild steel in 0.5 M HCl and 0.5 M NaCl the absence and presence of 10 ppm of different additives of nanoparticles

Medium	Additive	$R_s$ (ohm $cm^2$ )	$Q_1$ ( $\mu F$ $cm^{-2}$ )	$N_1$	$R_2$ (ohm $cm^2$ )	$Q_2$ ( $\mu F$ $cm^{-2}$ )	$R_{ct}$ (ohm $cm^2$ )	$N_2$	$W_R$
0.5 M HCl + 1% SDS	–	1.9	448	0.8	–	–	38.2	–	–
	ZnMnO	2.6	212	0.8	–	–	41.7	–	–
	ZnMnFeO	3.7	304	0.8	–	–	57.5	–	–
0.5 M NaCl + 1% SDS	–	7.9	$67 \times 10^{-4}$	0.6	95.0	$16 \times 10^{-4}$	3.3	1.0	$1.8 \times 10^{-6}$
	ZnMnO	5.8	$24 \times 10^{-4}$	0.6	1455	$21 \times 10^{-4}$	12.1	0.8	4.32
	ZnMnFeO	5.6	$25 \times 10^{-4}$	0.6	824	$10 \times 10^{-4}$	10.2	0.8	4.32

**Acknowledgments** The authors thank Dr. Mohamad Roumié the head of the accelerator Laboratory, Lebanese Atomic Energy Commission, CNRS, Beirut, Lebanon for the assistance in this work.

## Compliance with Ethical Standards

**Conflict of interests** The authors state that there are no conflicts of interest.

## References

- Hijazi KM, Abdel-Gaber AM, Younes GO (2015) Influence of *Malus domestica* and *Caesalpinia bonducella* Leaf Extracts on the Corrosion Behaviour of Mild Steel in  $H_2SO_4$  Solution. *Int J Electrochem Sci* 10:4779–4792
- El Hajjaji F, Salim R, Messali M, Hammouti B, Chauhan DS, Almutairi SM, Quraishi MA (2019) Electrochemical studies on new pyridazinium derivatives as corrosion inhibitors of carbon steel in acidic medium. *J Bio Tribo Corros* 5(1):4. <https://doi.org/10.1007/s40735-018-0195-3>
- Fouda AS, Migahed MA, Atia AA, Mousa IM (2016) Corrosion inhibition and adsorption behavior of some cationic surfactants on carbon steel in hydrochloric acid solution. *J Bio Tribo Corros* 2(4):22. <https://doi.org/10.1007/s40735-016-0052-1>
- Fouda AS, Megahed HE, Fouad N, Elbahrawi NM (2016) Corrosion inhibition of carbon steel in 1 M hydrochloric acid solution by aqueous extract of *thevetia peruviana*. *J Bio Tribo Corros* 2(3):16. <https://doi.org/10.1007/s40735-016-0046-z>
- Khadiri A, Ousslim A, Bekkouche K, Aouniti A, Warad I, Elidrissi A et al (2018) 4-(2-(2-(2-(Pyridine-4-yl) ethylthio) ethoxy) ethylthio) ethyl pyridine as new corrosion inhibitor for mild steel in 1.0 M HCl solution: experimental and theoretical studies. *J Biol Tribo Corros* 4(4):64. <https://doi.org/10.1007/s40735-018-0179-3>
- Anupama KK, Shainy KM, Joseph A (2016) Excellent anticorrosion behavior of *Ruta Graveolens* extract (RGE) for mild steel in hydrochloric acid: electro analytical studies on the effect of time, temperature, and inhibitor concentration. *J Bio Tribo Corros* 2(1):2–10
- Al-Moghrabi RS, Abdel-Gaber AM, Rahal HT (2018) A comparative study on the inhibitive effect of *Crataegus oxyacantha* and *Prunus avium* plant leaf extracts on the corrosion of mild steel in hydrochloric acid solution. *IJIC* 9(3):255–263
- Kadhim A (2018) Experimental investigation for corrosion inhibition of mild steel in hydrochloric acid bath by 3-[(5-phenyl-1,3,4-thiadiazol-2-yl) imino]-2-oxoindoline. *J Mater Sci: Mater Electron* 29(6):4683–4688
- Lata S, Chaudhary RS (2008) Some triphosphates as corrosion inhibitors for mild steel in 3% NaCl solution. *Indian J Chem Technol* 15:364–374
- Li WH, He Q, Zhang ST, Pei CL, Hou BR (2008) Some new triazole derivatives as inhibitors for mild steel corrosion in acidic medium. *J Appl Electrochem* 38(3):289–295
- Shainy KM, Ammal PR, Unni KN, Benjamin S, Joseph A (2016) Surface interaction and corrosion inhibition of mild steel in hydrochloric acid using pyoverdine, an eco-friendly bio-molecule. *J Bio Tribo Corros* 2(3):20–22
- Mohsenifar F, Jafari H, Sayin K (2016) Investigation of thermodynamic parameters for steel corrosion in acidic solution in the presence of N, N'-Bis (phloroacetophenone)-1, 2 propanediamine. *J Bio Tribo Corros* 2(1):1–3
- El-Rehim SA, Refaey SAM, Taha F, Saleh MB, Ahmed RA (2001) Corrosion inhibition of mild steel in acidic medium using 2-amino thiophenol and 2-cyanomethyl benzothiazole. *J Appl Electrochem* 31(4):429–435
- Selvi ST, Raman V, Rajendran N (2003) Corrosion inhibition of mild steel by benzotriazole derivatives in acidic medium. *J Appl Electrochem* 33(12):1175–1182
- Aspenes, G. (2010). The influence of pipeline wettability and crude oil composition on deposition of gas hydrates during petroleum production
- Atta AM, El-Mahdy GA, Allohedan HA (2013) Corrosion inhibition efficiency of modified silver nanoparticles for carbon steel in 1 M HCl. *Int J Electrochem Sci* 8(4):4873–4885
- Zubillaga O, Cano FJ, Azkarate I, Molchan IS, Thompson GE, Skeldon P (2009) Anodic films containing polyaniline and nanoparticles for corrosion protection of AA2024T3 aluminium alloy. *Surf Coat Technol* 203(10):1494–1501
- Gao G, Wu H, He R, Cui D (2010) Corrosion inhibition during synthesis of Cu<sub>2</sub>O nanoparticles by 1, 3-diaminopropane in solution. *Corros Sci* 52(9):2804–2812
- Zhang X, Wang F, Du Y (2007) Effect of nano-sized titanium powder addition on corrosion performance of epoxy coatings. *Surf Coat Technol* 201(16):7241–7245
- Atta AM, El-Azabawy OE, Ismail HS, Hegazy MA (2011) Novel dispersed magnetite core-shell nanogel polymers as corrosion inhibitors for carbon steel in acidic medium. *Corros Sci* 53(5):1680–1689
- Moussa D, Bakeer DES, Awad R, Abdel-Gaber AM (2017) Physical properties of ZnO nanoparticles doped with Mn and Fe. *IOP Publishing. J Phys Conf Ser* 869(1):012021
- Basma H, Roumié M, Awad R, Marhaba S, Albast M, Abualy A (2015) Ion beam analysis and electric properties of GdBa<sub>2</sub>Cu<sub>3</sub>O<sub>7-δ</sub> added with nanosized ferrites ZnFe<sub>2</sub>O<sub>4</sub> and CoFe<sub>2</sub>O<sub>4</sub>. *Mater Sci Appl* 6(09):828
- Anand K, Varghese S (2017) Role of surfactants on the stability of nano-zinc oxide dispersions. *Part Sci Technol* 35(1):67–70
- Rahal HT, Abdel-Gaber AM, Younes GO (2016) Inhibition of steel corrosion in nitric acid by sulfur containing compounds. *Chem Eng Commun* 203(4):435–445
- Gurbich AF (1997) Evaluation of non-Rutherford proton elastic scattering cross section for oxygen. *Nucl Instrum Methods Phys Res B* 129(3):311–316
- Ramos AR, Paul A, Rijniers L, Da Silva MF, Soares JC (2002) Measurement of (p, p) elastic differential cross-sections for carbon, nitrogen, oxygen, aluminium and silicon in the 500–2500 keV range at 140 and 178 laboratory scattering angles. *Nucl Instrum Methods Phys Res B* 190(1–4):95–99
- Abd-El-Khalek DE, Abdel-Gaber AM (2012) Evaluation of nicotiana leaves extract as corrosion inhibitor for steel in acidic and neutral chloride solutions. *Electrochim Acta* 30(4):247–259
- Abdel-Gaber AM, Abd-El Nabey BA, Sidahmed IM, El-Zayady AM, Saadawy M (2006) Effect of temperature on inhibitive action of damsisia extract on the corrosion of steel in acidic media. *Corrosion* 62(4):293–299
- Rahal HT, Abdel-Gaber AM, Awad R (2017) Corrosion behavior of a superconductor with different SnO<sub>2</sub> nanoparticles in simulated seawater solution. *Chem Eng Commun* 204(3):348–355
- Rahal HT, Abdel-Gaber AM, Awad R (2017) Influence of SnO<sub>2</sub> nanoparticles incorporation on the Electrochemical behaviour of a superconductor in sodium sulphate solutions. *Int J Electrochem Sci* 12:10115–10128

31. Abdel-Gaber AM, Abd-El-Nabey BA, Khamis E, Abd-El-Khalek DE (2008) Investigation of fig leaf extract as a novel environmentally friendly antiscalant for  $\text{CaCO}_3$  calcareous deposits. *Desalination* 230(1–3):314–328
32. Abdel-Gaber AM, Masoud MS, Khalil EA, Shehata EE (2009) Electrochemical study on the effect of Schiff base and its cobalt complex on the acid corrosion of steel. *Corros Sci* 51(12):3021–3024
33. Ahmad Z (2006) Principles of corrosion engineering and corrosion control. Elsevier, Boston

**Publisher's Note** Springer Nature remains neutral with regard to jurisdictional claims in published maps and institutional affiliations.